A model of the glycine receptor deduced from Brownian dynamics studies

Megan O'Mara*, Peter H. Barry†, and Shin-Ho Chung*‡

*Department of Theoretical Physics, Research School of Physical Sciences, Australian National University, Canberra 0200, Australia; and †Department of Physiology and Pharmacology, University of New South Wales, Sydney 2052, Australia

Communicated by Sidney Altman, Yale University, New Haven, CT, February 3, 2003 (received for review December 12, 2002)

We have developed a three-dimensional model of the α1 homomeric glycine receptor by using Brownian dynamics simulations to account for its observed physiological properties. The model channel contains a large external vestibule and a shallow internal vestibule, connected by a narrow, cylindrical selectivity filter. Three rings of charged residues from the pore-lining M2 domain are modeled as point charges in the protein. Our simulations reproduce many of the key features of the channel, such as the current–voltage profiles, permeability ratios, and ion selectivity. When we replace the ring of alanine residues lining the selectivity filter with glutamates, the mutant model channel becomes permeable to cations, as observed experimentally. In this mutation, anions act as chaperones for sodium ions in the extracellular vestibule, and together they penetrate deep inside the channel against a steep energy barrier encountered by unaccompanied ions. Two subsequent amino acid mutations increase the cation permeability, enabling monovalent cations to permeate through the channel unaided and divalent cations to permeate when chaperoned by anions. These results illustrate the key structural features and underlying mechanism for charge selectivity in the glycine receptor.

ligand-gated ion channels | conductance | permeation

In recent years, enormous strides have been made in our understanding of the structure-function relationships in biological ion channels. The determination of the structures of several different classes of ion channels and concurrent advances in computational biophysics have prompted numerous theoretical investigations that have shed considerable light on mechanisms of permeation and selectivity. Among these are the thermodynamics of cation permeation through the selectivity filter (1), macroscopic studies of energy profiles in the pore (2–4), semimicroscopic simulations to elucidate the mechanisms of ion permeation and selectivity (4–7), and molecular dynamics calculations focusing on permeation (8–14). In addition, three-dimensional Brownian dynamics simulations have been fruitfully used to construct a model of the L-type calcium channel (15, 16). These theoretical studies are reviewed in several recent articles (17–20).

One class of proteins that has been neglected in theoretical investigations is that of anion-selective channels. Important members of the ligand-gated anion channel family include the γ-aminobutyric acid (GABA) and glycine receptors, which mediate hyperpolarizing synaptic potentials in response to neurotransmitters. Although the crystal structures of the glycine and GABA receptors are not yet determined, the experimental findings and the high similarity of these channels to the nicotinic acetylcholine receptor allow us to make a reasonable conjecture on their approximate shape and the locations of dipoles and charged residues lining the channel wall. Like the acetylcholine receptor (21), which belongs to the same superfamily, the glycine receptor (GlyR) is likely to have a large extracellular vestibule connected to a narrow selectivity filter (22). The anion-selective α1 homomeric GlyR has two positively charged rings of arginine residues, one in the extracellular vestibule and one in the selectivity filter. There are also estimates of the minimum pore dimensions of the GlyR from a number of studies involving the use of permeant organic ions of different sizes (23, 24). Using the available information, we have constructed a model of the GlyR that replicates all of the available experimental data, including the results obtained from cation-selective mutant GlyRs.

Materials and Methods

We have constructed a three-dimensional model of the α1 homomeric GlyR from its experimental properties (23, 24) and primary structure (25, 26), used in conjunction with the basic topology of the acetylcholine receptor (21) and insights gathered from the crystal structure of the potassium channel. The resulting model, illustrated in Fig. 1*A*, extends asymmetrically across the membrane, with a large extracellular vestibule 57 Å in length and a smaller intracellular vestibule 17 Å long. Both vestibules have a mouth radius of 12.5 Å and taper down to join a narrow, cylindrical filter 6 Å long, with a radius of 3 Å. Three charged residues, one aspartate and two arginines, and a dipole representing the hydroxyl group of the threonine residue are placed along the wall of the model channel, 1 Å inside the protein, as indicated in Fig. 1*A*. We ascertained that moving these charges by 0.5 Å deeper inside the channel wall has negligible effect on the channel conductance. Because the GlyR is pentameric, the charges and dipoles are inserted five times, 72° apart. For example, a ring of five arginine residues is guarding the extracellular aspect of the narrow selectivity filter. The magnitude of charge on the threonine (T13′) dipole is held constant through all simulations at $\pm$ 0.375*e* (16) (where *e* is the unit charge of 1.6×10^{-19} C), with the positive end pointing toward the channel. The magnitude of charge on the other residues is varied systematically until the simulated conductance corresponds to the experimental values. This result occurs when aspartate (D-5′) carries a charge of $-0.25e$ and both arginine residues (R0′ and R19′) carry a charge of $+0.375e$.

The dielectric constant of the channel protein is taken as $\varepsilon_p = 2$ (3). To determine ε_w within narrow pores, one can either examine the interaction of the fluctuating dipole moment with a reaction field acting at the boundary or measure the induced polarization in response to an applied electric field. Neither method gives a reliable answer in narrow channels when ions are included. The value of ε_w can be estimated most accurately by equating the single or multiple ion potential of mean force from molecular dynamics to that found by solving Poisson's equation with assumed dielectric constants of water and protein. Meanwhile, we adopt the value of $\varepsilon_w = 60$. This value, when used in solving Poisson's equation, is found to closely reproduce the experimental conductance (5).

Using the α1 GlyR as a basis, we modeled two of the cation-selective mutations described in the literature (27, 28), which are characterized by systematic mutations of key amino acids residues in the M2 domain. The first of these mutant GlyRs contains a single point mutation of alanine to glutamate in the

Abbreviation: GlyR, glycine receptor.

‡To whom correspondence should be addressed. E-mail: shin-ho.chung@anu.edu.au.

 www.pnas.org/cgi/doi/10.1073/pnas.0630652100

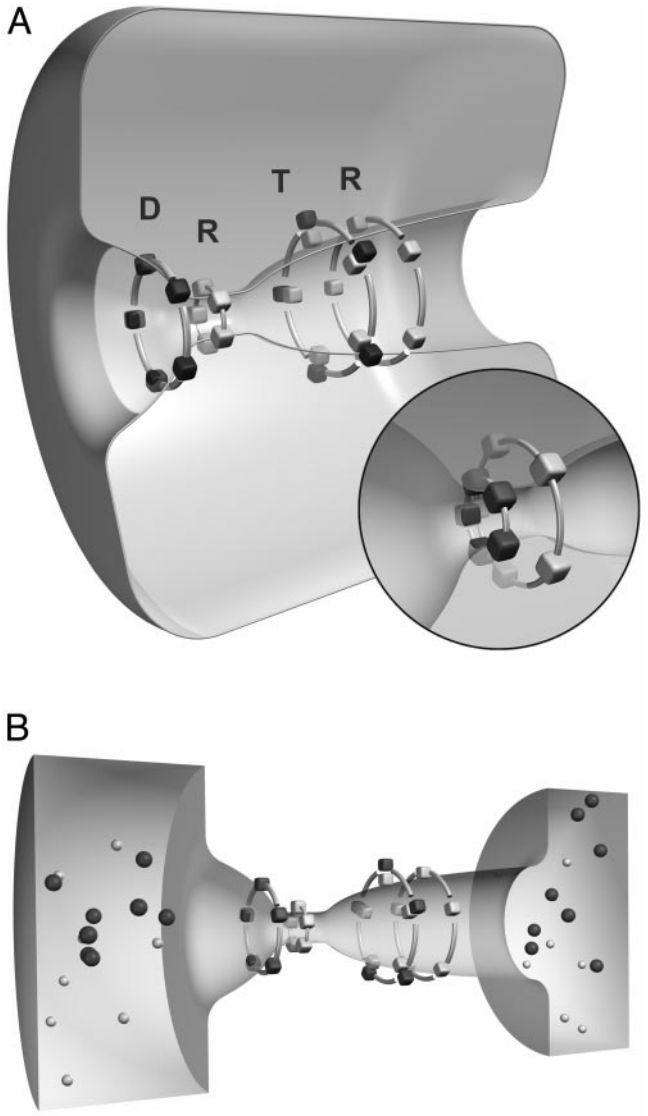

Fig. 1. A model of the α1 GlyR and the simulation system. (*A*) A cross section of the three-dimensional model shows two vestibules connected to a cylindrical selectivity filter. The extracellular space is on the right. The channel extends from $z = -40$ to 40 Å. The positions of the five groups of aspartate (D), arginine (R), threonine (T), and arginine (R) residues are marked by the small cubes and situated at $z = -29$, -21.5, -2, and 7 Å, respectively. Negative charges are represented by filled cubes and positive charges are represented by open cubes. In the first of the two of the mutant channels, a ring of glutamates is inserted in the selectivity filter, adjacent to the ring of arginine residues, and the arginines are moved 4 Å deeper into the protein, as shown in *Inset*. The triple mutant has an additional deletion of a ring of proline residues located in the selectivity filter and substitution of the outer ring of arginine residues for glutamates. (*B*) For Brownian dynamics simulations, the model GlyR is connected to two cylindrical reservoirs, representing the extracellular and intracellular spaces, and a fixed number of Na^+ and Cl^- ions are placed in each reservoir.

channel's selectivity filter (A-1′E), rendering the channel cation-selective. We carry out an analogous mutation on our model by inserting a ring of glutamate residues along the wall of the selectivity filter and moved the adjacent ring of arginine residues 4 Å deeper into the protein to reproduce the experimental anion to cation permeability ratio (27), as illustrated in Fig. 1*A Inset*. As the permeant cation studies show, this mutation has a slightly wider selectivity filter, with a radius of 3.25 Å (27); we increase the radius of the model selectivity filter accordingly. The subsequent deletion of a proline residue in the selectivity filter and substitution of glutamate for arginine in the extracellular vestibule (P-2Δ, A-1′E, R19′E) are sufficient to allow calcium permeation, giving a calcium-selective GlyR (triple mutant GlyR). This triple mutant is modeled by incorporating the arginine to glutamate substitution in the extracellular vestibule into the single mutant model. The proline deletion is expected to increase the selectivity filter radius. Permeant cation studies estimate the minimum pore radius to be 4.15 Å (27). However, because the precise structural alterations caused by such a mutation are unknown, our strategy is to vary the radius of the selectivity filter systematically between 3.0 and 4.15 Å, until the current–voltage curve derived from simulations matches that obtained experimentally, while preserving the other experimental properties of this mutant channel, such as its ability to conduct calcium ions. The charges assigned to each residue are varied systematically to produce currents that best fit the experimental data. For the single mutant GlyR, optimal conductances are obtained when D-5′ carries a charge of $-0.25e$, R0′ is set at $0.5e$, E-1′ is $-0.5e$, and R19′ is $0.25e$. The triple mutant carries a charge of $-0.5e$ on D-5′, $+0.625e$ on R0′ and $-0.625e$ on E-1′, and $-0.375e$ on E19′.

The electrostatic potential energy profile for various ion configurations in the channel is calculated from the numerical solutions of Poisson's equation by using the boundary element method (29). Energies of multiple ion systems are calculated with a steepest descent algorithm (3). To confirm the qualitative pictures gleaned from the energy profiles, we carry out three-dimensional Brownian dynamics simulations. In these simulations we solve the Langevin equation

$$m_i \frac{d\mathbf{v}_i}{dt} = -m_i\gamma_i\mathbf{v}_i + \mathbf{F}_i^R + q_i\mathbf{E}_i + \mathbf{F}_i^S, \qquad [1]$$

where m_i, v_i, $m_i\gamma_i$, and q_i are the mass, velocity, friction coefficient, and charge on an ion with index i, whereas $\mathbf{F}_i^R$, $\mathbf{E}_i$, and $\mathbf{F}_i^S$ are the random stochastic force, systematic electric field, and short range forces experienced by the ion, respectively. The Langevin equation is solved with the algorithm of van Gunsteren and Berendsen (30), by using the techniques described elsewhere (3, 31, 32). Electrostatic forces are determined by solving Poisson's equation with the boundary sector method (33), employing lookup table techniques (29, 35). To simulate the effects of short-range forces, we employ a multiple time-step algorithm, where a short time-step of 2 fs is used in the narrow selectivity filter and a long time-step of 100 fs is used in the outer and inner vestibules and reservoirs. The short-range forces we employ in the pore ($-23 \leq z \leq 17$ Å) include the Born energy barrier, an ion–ion interaction, and a repulsive ion–protein interaction similar to that described by Chung *et al.* (3). The ion–ion interaction consists of a long-ranged Coulomb term, and a short-ranged term that includes the influence of hydration waters, which will have some bearing on relative ion positions within the channel. Bulk ionic diffusion coefficients of 1.33×10^{-9} $m^2 \cdot s^{-1}$ for Na^+ and 2.03×10^{-9} $m^2 \cdot s^{-1}$ for Cl^- ions are used in the reservoirs and vestibules. These values are reduced to 50% of the bulk values in the selectivity filter (35). Simulations under various conditions, each lasting 1.6–10.0 μs, are performed with symmetric concentrations, generated with eight Na-Cl ion pairs in each reservoir. The reservoirs are connected to each end of the channel and have a set radius of 30 Å, as shown in Fig. 1*B*. The height of each reservoir is adjusted to give the desired concentration. With the exception of the anion to cation permeability ratios, 150 mM NaCl is used in all simulations and maintained with a stochastic boundary (3). A transmembrane potential is generated by introducing an electric field into the solution of Poisson's equation, as described elsewhere (31).

The anion to cation permeability ratio is calculated for each model GlyR, and the calcium to sodium permeability ratio is calculated for the triple mutant GlyR. To determine the anion to cation permeability ratios, Brownian dynamics simulations are performed by using solutions of 200 mM NaCl in the intracellular reservoir and 100 mM NaCl in the extracellular reservoir. The calcium to sodium permeability ratio is determined by using 50 mM NaCl and 50 mM $CaCl_2$ for the extracellular solution and 150 mM NaCl in the intracellular solution. The intracellular solution is doped with a single Ca^{2+} ion to avoid problems with the stochastic boundaries (3). The reversal potential of each current–voltage relationship is used in the Goldman–Hodgkins–Katz equation to derive the relevant permeability ratio.

Results

The electrostatic potential energy profiles for various ion configurations in the α1 GlyR is given in Fig. 2*A*. A Cl^- ion entering an empty channel falls into a deep energy well of 16 kT (1 kT = 4.11×10^{-21} J) created by the positively charged residues in the protein wall (lower solid line). In contrast, a Na^+ ion attempting to enter the pore will face an energy barrier of 27 kT (upper solid line), effectively excluding it from the channel. When one Cl^- ion resides in the selectivity filter, a second Cl^- ion entering from the right meets a much smaller well (dashed line), whose maximum depth of 12.4 kT occurs at the axial position of $z = 5$ Å. The incoming ion coexists in a stable equilibrium with the first ion, which resides in the selectivity filter at the position indicated by the arrow. The two-ion equilibrium is disrupted when a third ion enters the channel. The energy well created by the charged moieties is effectively eliminated by the three resident ions, and the inner-most Cl^- ion encounters an energy barrier of only ≈2 kT in the intracellular vestibule. The ion can easily surmount this shallow residual barrier through its random motions, allowing it to move freely into the intracellular reservoir. Thus, conduction across the α1 GlyR takes place when the channel cradles three resident ions.

Fig. 2*B* shows the distribution of ions in the channel. The channel is divided into 80 sections, 1 Å in length, and the average number of ions in each section during a 0.2-μs simulation is plotted. With an applied voltage of +60 mV (inside positive with respect to outside), there are two prominent peaks in the histogram, one at $z = -20$ Å and the other at $z = 6$ Å. There are, on average, 0.97 ions in the selectivity filter and 1.9 ions in the extracellular vestibule of the channel. Assisted by the Coulomb repulsive force, the innermost ion is ejected into the intracellular reservoir when an ion from the extracellular vestibule stumbles into the selectivity filter. This process is the rate-limiting step in conduction of the GlyR. By counting the number of ions that traverse the channel in a fixed simulation period, we can deduce the magnitude of current at a fixed applied potential. In Fig. 2*C* we display the current–voltage relationship derived from Brownian dynamics simulations (filled circles). The current–voltage relationship is linear when the applied potential is between ±40 mV, but deviates slightly from Ohm's law at ±60 mV. The simulated currents are slightly smaller in magnitude than the experimental values at ±60 mV. The core conductance, derived by fitting a linear regression through the data points, is 66 pS. The experimental currents obtained from α1 GlyR expressed in human embryonic kidney cells (27) are superimposed on the simulated results. There is a close agreement between the simulated and experimental points. The simulated currents tend to increase linearly as a function of Cl^- activity up to 350 mM, but no experimental measurements of current–concentration relationships for the α1 GlyR are available for comparison. To test our model further, we calculate the permeability ratio of Cl^- ions to Na^+ ions by using the method described by Keramidas *et al.* (27). The simulated anion to cation permeability ratio is

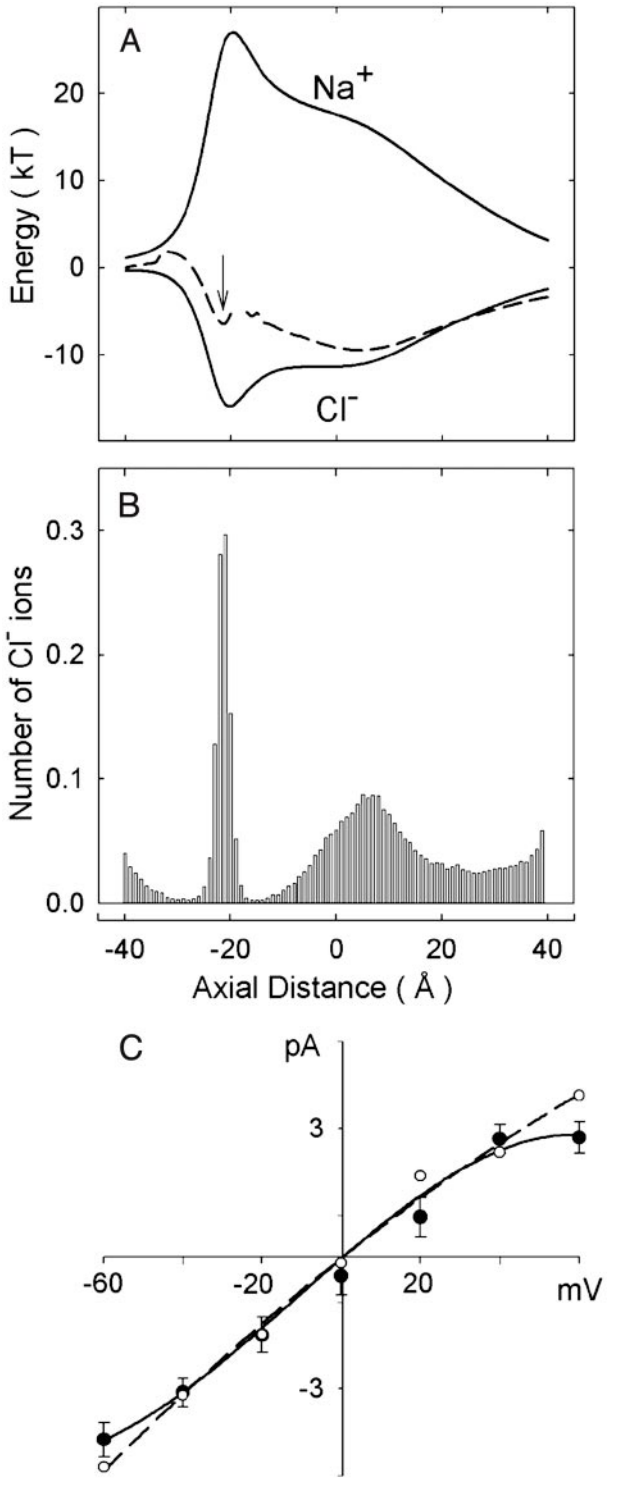

Fig. 2. Properties of the model GlyR deduced from electrostatic calculations and Brownian dynamics simulations. (*A*) The energy profiles encountered by a Na^+ ion (upper solid line) and a Cl^- ion (lower solid line) are illustrated. The profile encountered by a second Cl^- ion entering the channel from the extracellular space, with one Cl^- ion resident in the selectivity filter (at the axial position $z = -20$ Å, indicated by the arrow) is shown in the middle (broken line). (*B*) A dwell histogram indicates the region of the channel where Cl^- ions preferentially reside. The channel is divided into 80 sections, and the average number of ions in each slice is counted during a simulation period of 1 μs. (*C*) The simulated current–voltage relationship obtained from the model GlyR (filled circles) is compared with that obtained experimentally. Simulated error bars have a length of one standard error of the mean in this and subsequent figures and are not shown when they are smaller than the data points.

33.7 ± 1.0, which concurs with the experimental values of 24.6 ± 0.7 (36) and 27.9 ± 1.3 (27).

Our model of the GlyR should also reproduce the experimental observations obtained from mutant GlyRs. When the ring of alanine residues lining the selectivity filter is replaced with glutamate residues (A-1′E), the mutant channel becomes predominantly permeable to Na^+ ions (27). Fig. 3*A* shows the energy profiles encountered by a Na^+ ion (broken line) and Cl^- ion (solid line) traversing the channel along the central axis. On initial inspection, the single mutant GlyR seems to be impermeable to both anions and cations: a Cl^- ion attempting to move from the extracellular to the intracellular space must overcome a barrier of 21 kT to cross the selectivity filter, whereas a Na^+ ion must overcome a barrier of 10 kT to enter the extracellular vestibule. These barriers are generally insurmountable, but simulations reveal that substantial numbers of Na^+ ions move across the mutant GlyR, as shown in the current–voltage curve in Fig. 3*B*. The mutant GlyR is outwardly rectifying and the current at +60 mV is 1.02 pA. In accordance with the simulated results, the experimental data shows this single mutation switches selectivity of the GlyR from anions to cations. The simulated and experimental anion to cation permeability ratios support this finding, with values of 0.17 ± 0.02 and 0.34 ± 0.02 (27), respectively. Because the cationic current is small, the full current–voltage relationship obtained from single channel recordings is not yet available in the literature. The shape of the curve obtained from whole-cell configurations (27, 28), nevertheless, is broadly similar to that shown in Fig. 3*B*. However, there are experimentally determined single-channel currents at −60 mV and +60 mV of 0.66 ± 0.06 and 0.42 ± 0.03 pA. The corresponding simulated values we obtained are 1.02 ± 0.06 and 0.48 ± 0.03 pA.

The reason for the finite conductance is as follows: cations are able to move across the extracellular vestibule of the single mutant GlyR only when they are chaperoned by counterions. The ring of threonine dipoles and the outer ring of the arginine residues allow Cl^- ions to penetrate deep into the extracellular vestibule. In the selectivity filter, the ring of glutamate residues is closer to the pore than the arginine ring, overwhelming its effect. This result creates an energy barrier for Cl^- ions, excluding them from the selectivity filter. In the extracellular vestibule, a Cl^- ion closely accompanying a Na^+ ion neutralizes the effective charge, thus obliterating the barrier seen by a lone Na^+ ion. Once a Na^+ ion reaches the outer segment of the selectivity filter, it falls into a deep energy well created by the glutamate residues, leaving its chaperoning Cl^- ion behind. The dwell histograms for Cl^- (open bars) and Na^+ ions (filled bars) shown in Fig. 3*C* confirm the qualitative account of the dynamic interactions between the permeating cation and a counterion observed from video animations. On average, there are 2.1 Cl^- ions in the external vestibule, but none enter the cylindrical selectivity filter. There are also, on average, 2.1 Na^+ ions in the pore, residing predominantly in the selectivity filter and the internal vestibule. An occasional Na^+ stumbling into the external vestibule is quickly captured by one of the resident Cl^- ions and together they drift inward. When Cl^- ions are prevented from entering the vestibule by erecting an arbitrary barrier at the vestibule mouth, conduction across the single mutant GlyR ceases. Wang *et al.* (37) reported similar anion–cation interactions in mutated γ-aminobutyric acid-gated Cl^- channels.

In the case of the triple mutant GlyR, the substituted ring of negatively charged glutamate residues renders the extracellular vestibule inhospitable to anions, indicating that Na^+ conduction is not chaperoned. To account for a structural change after the proline deletion, we systematically increase the channel radius from 3.0 to 4.15 Å and observed the effects on both the Ca^{2+} permeation and NaCl current–voltage relationship. Fig. 4*A* shows the current–voltage relationships obtained from two triple

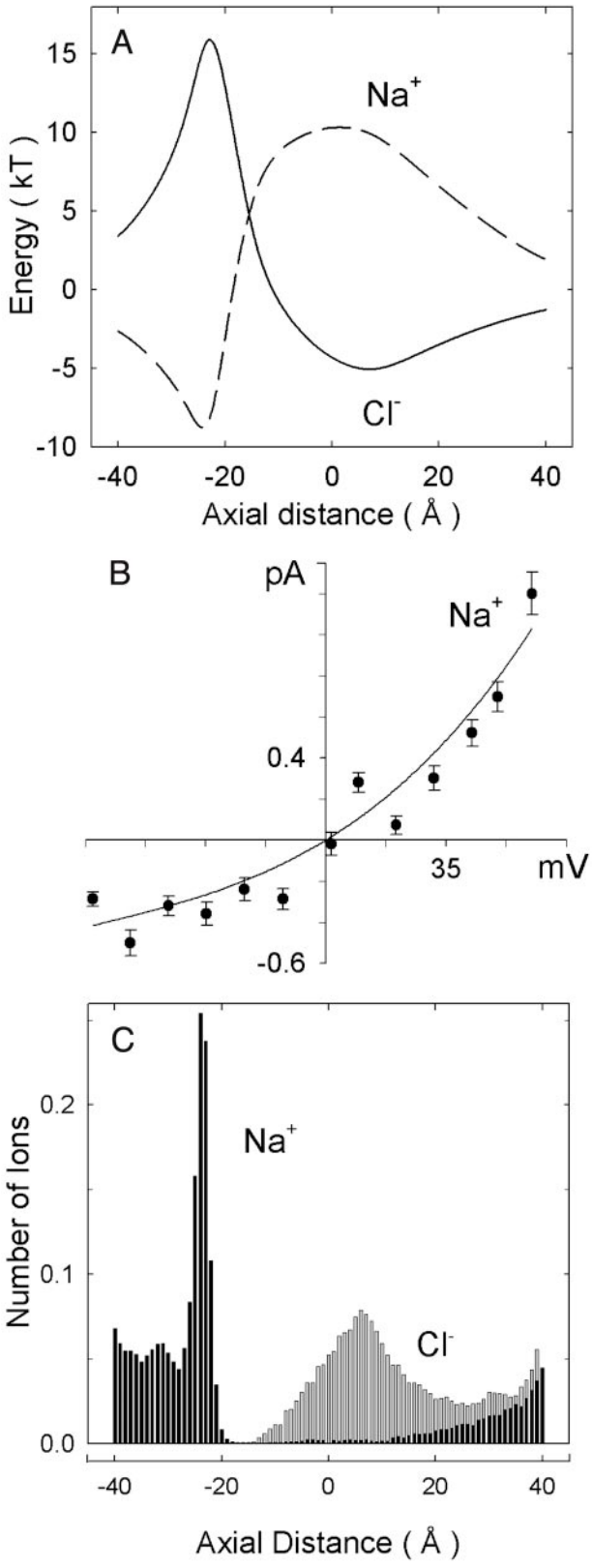

Fig. 3. Properties of the single mutant GlyR. A ring of five glutamate residues is inserted at the position indicated in Fig. 1*A Inset*. (*A*) The energy profiles seen by a single Cl^- ion (solid line) and a single Na^+ ion (broken line) are illustrated. (*B*) The current–voltage relationship shows that the channel is outwardly rectifying. (*C*) Dwell histograms of Na^+ ions (filled bars) and Cl^- ions (open bars) reveal that the external vestibule is occupied by, on average, two anions, whereas the selectivity filter is occupied by one Na^+ ion.

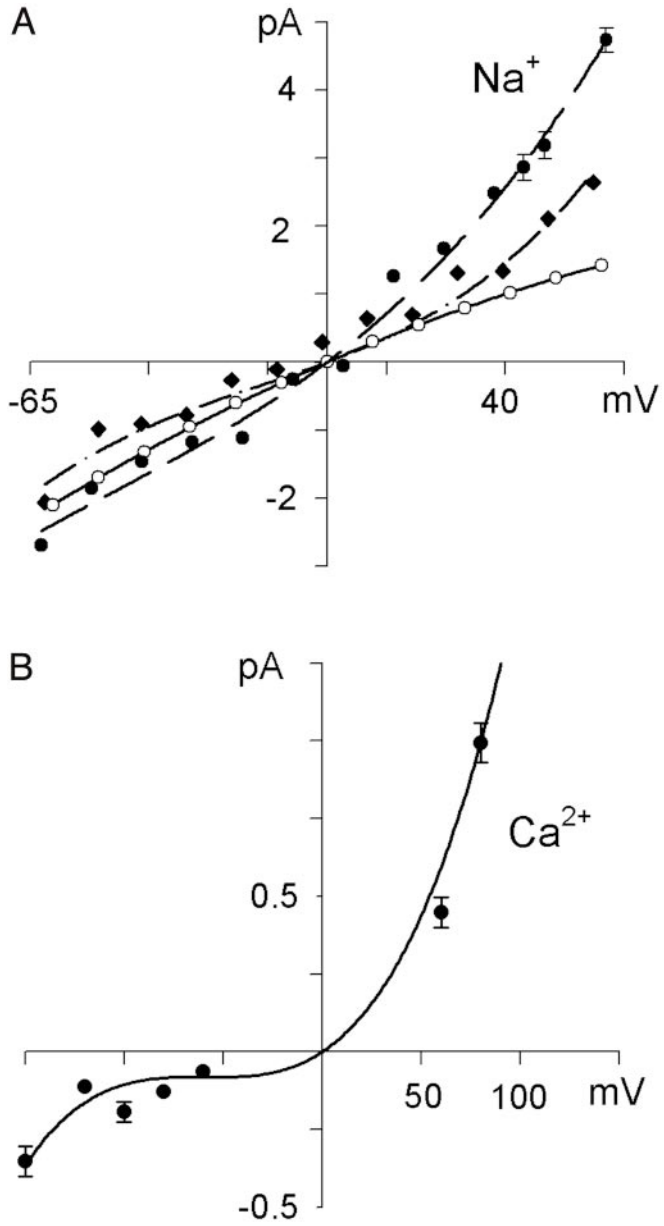

Fig. 4. The current–voltage relationships obtained from the triple mutant GlyR. A ring of five proline residues lining the selectivity filter is deleted. In addition, five glutamate residues are inserted in the position indicated in Fig. 1*A Inset*, and the arginine residues in the external vestibule are replaced by glutamate residues. (*A*) The NaCl current–voltage curves obtained with the radius of the selectivity filter fixed at 4.15 Å (filled circles) and 3.80 Å (filled diamonds) are superimposed on the experimental data (open circles). (*B*) The $CaCl_2$ current–voltage relationship still exhibits outwards rectification and currents approximately one-third the magnitude seen for NaCl.

mutant GlyR models with different selectivity filter radii. When the radius of the narrow segment is fixed at 4.15 Å (filled circles), the simulated currents are consistently higher than the experimental values (open circles). At an applied potential of +60 mV, the simulated current is 4.3 pA, compared with the experimental value of 1.4 pA. When the radius is reduced to 3.8 Å, the simulated currents (filled diamonds) are closer to the experimental values. The inward currents are slightly less and the outward currents slightly more than the measured currents. At applied potentials of +50 and +60 mV, the discrepancies become somewhat accentuated. As we continue to decrease the radius of the pore below 3.8 Å, the channel becomes impermeable to Ca^{2+} ions. In 150 mM $CaCl_2$, the current–voltage relationship also shows a pronounced outwards rectification at positive voltages, as seen in Fig. 4*B*, but the currents involved are less than one third the currents obtained for NaCl and similar in magnitude to those obtained in the single mutant GlyR current–voltage relationship. Further investigations show that calcium permeation in the triple mutant GlyR is analogous to sodium permeation in the single mutant GlyR: the presence of a Ca^{2+} ion in the selectivity filter alters the charge distribution in the triple mutant GlyR, attracting Cl^- ions into the extracellular vestibule. When a subsequent Ca^{2+} ion enters the extracellular vestibule, the energy barrier experienced by the incoming Ca^{2+} ion is diminished by the presence of the Cl^- ion, which chaperones the Ca^{2+} to the mouth of the selectivity filter. As a further test of our model, we measure the anion to cation and the Ca^{2+} to Na^+ permeability ratio of the triple mutant GlyR. Despite the outwards rectification in the current–voltage relationship, the simulated and experimental anion to cation permeability ratios concur, with ratios of 0.25 ± 0.02 and 0.19 ± 0.02, respectively. The simulated calcium to sodium permeability ratio of 0.76 ± 0.01 is also in close agreement with the experimental ratio of 0.92 ± 0.02.

Concluding Remarks

Our model of the GlyR successfully reproduces the experimentally observed conductances, anion to cation permeability ratios, and current–voltage profiles in the wild-type and mutant α1 homomeric GlyRs. This result suggests that our model contains many of the important features that regulate ion permeation across the GlyR. Brownian dynamics simulations have shed light on the mechanism of ion permeation in the three mutations studied, illustrating both unaided and chaperoned ion permeation. While the search for the complete tertiary structures of the ligand-gated ion channels continues, useful insights to the pore structure and permeation mechanism may be obtained from a study of the inverse problem, that is, predicting relevant aspects of the channel structure from its functional properties.

The success of our technique of constructing models of ion channels whose crystal structures are unknown, such as L-type calcium channels (15, 16), diverse ranges of potassium channels (7), and the GlyR as reported here, has prompted studies of other ion channels, including the voltage-gated sodium channel and other members of the ligand-gated ion channel family.

All calculations were carried out on the Fujitsu VPP-300 and the Compaq AlphaServer Supercomputer of the Australian National University Supercomputer Facility. We thank Angelo Keramidas and Andrew Moorhouse for discussions and for making their experimental results available to us. This work was supported by grants from the Australian Research Council and the National Health and Medical Research Council of Australia.

1. Garofoli, S. & Jordan, P. C. (2003) *Biophys. J.*, in press.
2. Roux, B. & MacKinnon, R. (1999) *Science* **285,** 100–102.
3. Chung, S.-H., Allen, T. W., Hoyles, M. & Kuyucak. S. (1999) *Biophys. J.* **77,** 2517–2533.
4. Chung, S.-H., Allen, T. W. & Kuyucak, S. (2002) *Biophys. J.* **82,** 628–645.
5. Allen, T. W. & Chung, S.-H. (2001) *Biochim. Biophys. Acta* **1515,** 83–91.
6. Burykin, A., Schutz, C. N., Villá, J. & Warshel, A. (2002) *Proteins* **47,** 265–280.
7. Chung, S.-H., Allen, T. W. & Kuyucak, S. (2002) *Biophys. J.* **83,** 263–277.
8. Allen, T. W., Hoyles, M., Kuyucak, S. & Chung, S.-H. (1999) *Chem. Phys. Lett.* **313,** 358–365.
9. Allen, T. W., Kuyucak, S. & Chung, S.-H. (1999) *Biophys. J.* **77,** 2502–2516.
10. Bernèche, S. & Roux, B. (2000) *Biophys. J.* **78,** 2900–2917.
11. Åqvist, J. & Luzhkov, V. B. (2000) *Nature* **404,** 881–884.
12. Shrivastava, I. H. & Sansom, M. S. P. (2000) *Biophys. J.* **78,** 557–570.
13. Luzhkov, V. B. & Åqvist, J. (2000) *Biochim. Biophys. Acta* **1481,** 360–370.

14. Biggin, P. C., Smith, G. R., Shrivastava, I., Choe, S. & Sansom, M. S. P. (2001) *Biochim. Biophys. Acta* **1510,** 1–9.
15. Corry, B., Allen, T. W., Kuyucak, S. & Chung, S.-H. (2000) *Biochim. Biophys. Acta* **1509,** 1–6.
16. Corry, B., Allen, T. W., Kuyucak, S. & Chung, S.-H. (2001) *Biophys. J.* **80,** 195–214.
17. Tieleman, D. P., Biggin, P. C., Smith, G. R. & Sansom, M. S. P. (2001) *Q. Rev. Biophys.* **34,** 473–561.
18. Kuyucak, S., Andersen, O. S. & Chung, S.-H. (2001) *Rep. Prog. Phys.* **64,** 1427–1472.
19. Chung, S.-H. & Kuyucak, S. (2002) *Eur. Biophys. J.* **31,** 283–293.
20. Chung, S.-H. & Kuyucak, S. (2002) *Biochim. Biophys. Acta* **1565,** 267–286.
21. Unwin, N. (1993) *Cell* **72,** Suppl., 31–41.
22. Lester, H. J. (1992) *Annu. Rev. Biophys. Biomol. Struct.* **21,** 267–292.
23. Bormann, J., Hamill, O. P. & Sakmann, B. (1987) *J. Physiol.* **385,** 243–286.
24. Fatima-Shad, K. & Barry, P. H. (1993) *Proc. R. Soc. London Ser. B* **253,** 69–75.
25. Bormann, J., Runström, N., Betz, H. & Langosch, D. (1993) *EMBO J.* **12,** 3729–3737.
26. Langosch, D., Thomas, L. & Betz, H. (1988) *Proc. Natl. Acad. Sci. USA* **85,** 7394–7398.
27. Keramidas, A., Moorhouse, A. J., Pierce, K. D., Schofield, P. R. & Barry, P. H. (2002) *J. Gen. Physiol.* **119,** 393–410.
28. Moorhouse, A. J., Keramidas, A., Zaykin, A., Schofield, P. R. & Barry, P. H. (2002) *J. Gen. Physiol.* **119,** 411–425.
29. Hoyles, M., Kuyucak, S. & Chung, S.-H. (1998) *Phys. Rev. E* **58,** 3654–3661.
30. van Gunsteren, W. F., Berendsen, H. J. C. & Rullmann, J. A. (1981) *Mol. Phys.* **44,** 69–95.
31. Li, S., Hoyles, M., Kuyucak, S. & Chung, S.-H. (1998) *Biophys. J.* **74,** 37–47.
32. Chung, S.-H., Hoyles, M., Allen, T. W. & Kuyucak, S. (1998) *Biophys. J.* **75,** 793–809.
33. Hoyles, M., Kuyucak, S. & Chung, S.-H. (1996) *Biophys. J.* **70,** 1628–1642.
34. Hoyles, M., Kuyucak, S. & Chung, S.-H. (1998) *Comput. Phys. Commun.* **115,** 45–68.
35. Allen, T. W., Chung, S.-H. & Kuyucak, S. (2000) *Biophys. Chem.* **86,** 1–14.
36. Keramidas, A., Moorhouse, A. J., French, C. R., Schofield, P. R. Barry, P. H. (2000) *Biophys. J.* **78,** 247–259.
37. Wang, C.-T., Zhang, H.-G., Rocheleau, T. A., ffrench-Constant, R. H. & Jackson, M. B. (1999) *Biophys. J.* **77,** 691–700.